Check for updates

ADVANCED MATERIALS
www.advmat.de

A Thermally Activated Delayed Fluorescence Green OLED with 4500 h Lifetime and 20% External Quantum Efficiency by Optimizing the Emission Zone using a Single-Emission Spectrum Technique

Rossa Mac Ciarnáin, Hin Wai Mo, Kaori Nagayoshi, Hiroshi Fujimoto, Kentaro Harada, Robert Gehlhaar, Tung Huei Ke, Paul Heremans, and Chihaya Adachi**

Device optimization of light-emitting diodes (LEDs) targets the most efficient conversion of electrically injected charges into emitted light. The emission zone in an LED is where charges recombine and light is emitted from. It is believed that the emission zone is strongly linked to device efficiency and lifetime. However, the emission zone size is below the optical diffraction limit, so it is difficult to measure. An accessible method based on a single emission spectrum that enables emission zone measurements with sub-second time resolution is shown. A procedure is introduced to study and control the emission zone of an LED system and correlate it with device performance. A thermally activated delayed fluorescence organic LED emission zone is experimentally measured over all luminescing current densities, while varying the device structure and while ageing. The emission zone is shown to be finely controlled by emitter doping because electron transport via the emitter is the charge-transport bottleneck of the system. Suspected quenching/degradation mechanisms are linked with the emission zone changes, device structure variation, and ageing. Using these findings, a device with an ultralong 4500 h T_{95} lifetime at 1000 cd m^{-2} with 20% external quantum efficiency is shown.

1. Introduction

Today, commercial organic light emitting diodes (OLEDs) generally feature low efficiency, blue fluorescent emitters with green and red phosphorescent emitters containing the rare iridium metal which is expensive and environmentally destructive to obtain.[1,2] Conversely, purely organic thermally activated delayed fluorescence (TADF) emitters offer lower production costs and efficient red, green, and blue emitters. However, they have not been shown to have sufficient device lifetime.[3,4] In this article, it is shown that optimization of the location of the emission zone is correlated with increasing the operational lifetime of TADF OLEDs. The OLED system studied in this work uses, as a starting point, an established OLED stack[5] featuring the green 2,4,5,6-tetrakis(carbazol-9-yl)-1,3-dicyanobenze (4CzIPN) TADF emitter (see **Figure 1**d).

This work is based on a well-established optical model for OLED emission,[6–8] but an adapted methodology is presented. Using our optical results together with results from literature degradation studies, reasons for the device degradation are hypothesized. The goal of this work was to find a more directed approach to OLED stack optimization. The optical measurement procedure introduced gives an experimental visualization of the OLED emission zone (EZ), without requiring knowledge of difficult to determine electrical parameters, as used for electrical charge dynamics simulations of organic semiconductor systems.

OLEDs operate on the basis of controlled recombination of injected charge carriers (called electrons or holes for convenience). Electrons and holes in organic films are radical anions or radical cations, respectively, and are doublets in terms of spin dynamics. The radical state appears to move together with its polarization cloud because it polarizes the orbitals of the surrounding neutral molecules and it may also be subject to an intramolecular vibrational relaxation.[9] Such a quasistatic formation is called a polaron. Intrinsically long-lived triplet excited states of emitter molecules and their interactions with polarons

R. Mac Ciarnáin, R. Gehlhaar, T. H. Ke, P. Heremans
imec
Kapeldreef 75, Leuven B3001, Belgium
E-mail: rossa.macciarnain@imec.be
R. Mac Ciarnáin, P. Heremans
KU Leuven
Kasteelpark Arenberg 10, Leuven B3001, Belgium
H. W. Mo, K. Nagayoshi, H. Fujimoto, K. Harada, C. Adachi
i^3-opera
5-14 Kyudai-shimmachi, Nishi, Fukuoka 819-0388, Japan
E-mail: adachi@cstf.kyushu-u.ac.jp
H. Fujimoto, K. Harada, C. Adachi
OPERA Research Group
Kyushu University
744 Motooka, Nishi, Fukuoka 819-0395, Japan

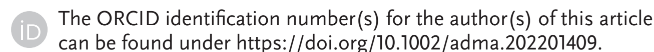
The ORCID identification number(s) for the author(s) of this article can be found under https://doi.org/10.1002/adma.202201409.

© 2022 The Authors. Advanced Materials published by Wiley-VCH GmbH. This is an open access article under the terms of the Creative Commons Attribution-NonCommercial-NoDerivs License, which permits use and distribution in any medium, provided the original work is properly cited, the use is non-commercial and no modifications or adaptations are made.

DOI: 10.1002/adma.202201409

 © 2022 The Authors. Advanced Materials published by Wiley-VCH GmbH

15214095, 2022, 29, Downloaded from https://onlinelibrary.wiley.com/doi/10.1002/adma.202201409 by EVIDENCE AID - BELGIUM, Wiley Online Library on [21/12/2022]. See the Terms and Conditions (https://onlinelibrary.wiley.com/terms-and-conditions) on Wiley Online Library for rules of use; OA articles are governed by the applicable Creative Commons License

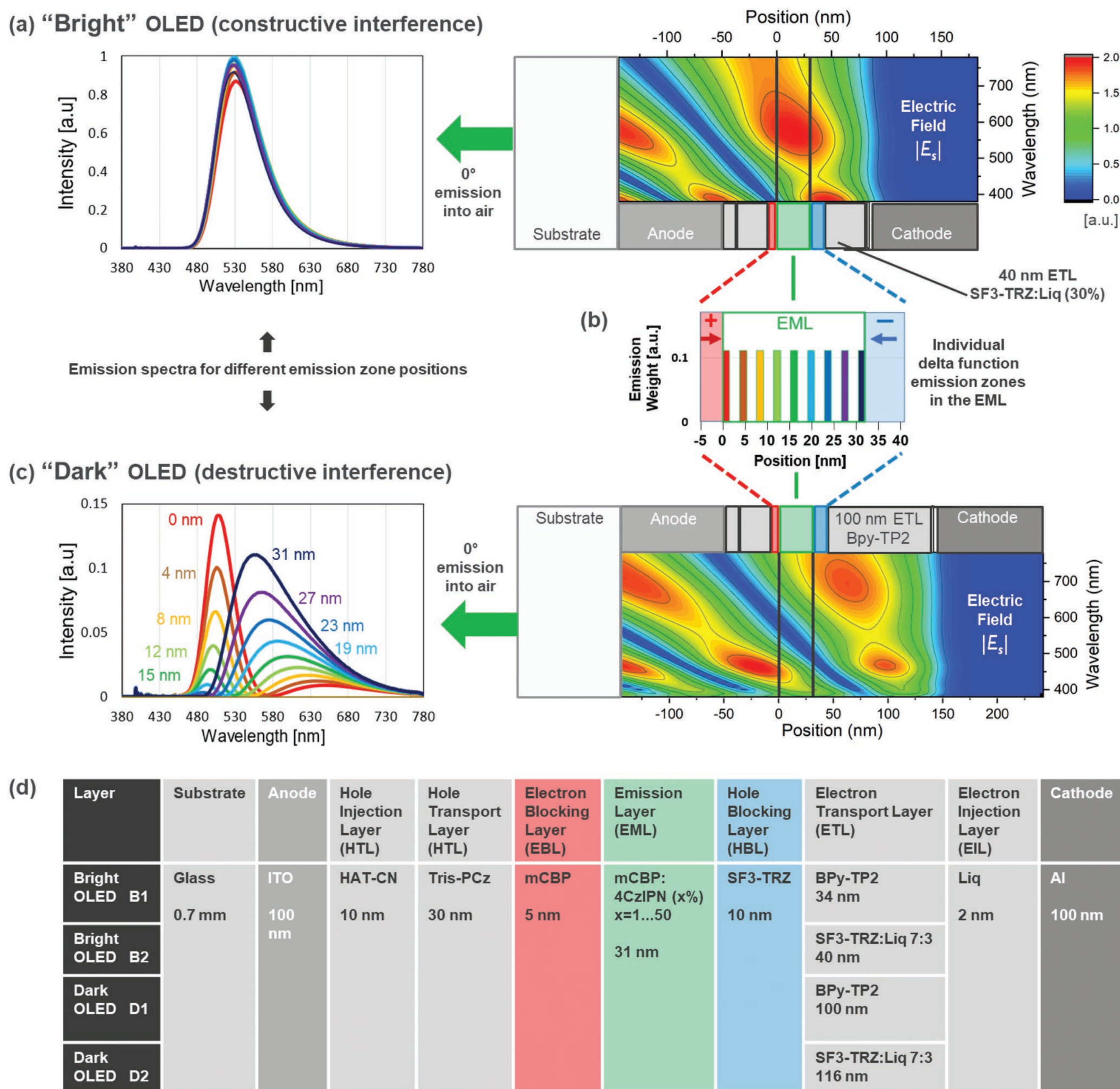

Layer	Substrate	Anode	Hole Injection Layer (HTL)	Hole Transport Layer (HTL)	Electron Blocking Layer (EBL)	Emission Layer (EML)	Hole Blocking Layer (HBL)	Electron Transport Layer (ETL)	Electron Injection Layer (EIL)	Cathode
Bright OLED B1	Glass 0.7 mm	ITO 100 nm	HAT-CN 10 nm	Tris-PCz 30 nm	mCBP 5 nm	mCBP: 4CzIPN (x%) x=1...50 31 nm	SF3-TRZ 10 nm	BPy-TP2 34 nm	Liq 2 nm	Al 100 nm
Bright OLED B2								SF3-TRZ:Liq 7:3 40 nm		
Dark OLED D1								BPy-TP2 100 nm		
Dark OLED D2								SF3-TRZ:Liq 7:3 116 nm		

Figure 1. a) Left: Emission spectra for the individual EZ positions defined in (b); right: The electric field modes for bright, device B2 which gives constructive interference of the standing-wave in the EML.[6] The microcavity electric field enhancement (Discussion S2, Supporting Information) representing 0° emission is shown. For (a), a standard constructive interference bright OLED, the emission spectrum is quite insensitive to the EZ position. b) Nine individual infinitely thin emission zones at different positions in the EML, with 3.9 nm spacing. c) As in (a) but for a thicker ETL dark device D1 giving, this time, destructive interference of the standing wave in the EML. d) OLED layer materials and thicknesses. Different ETL materials can give comparable current–voltage curves for bright and dark devices of different ETL thickness devices, for example, B2 and D1. Due to the differing refractive indices, the bright device ETL thicknesses are different for each material to give the same optical path and interference conditions. In the destructive interference microcavity EZ measurement method, the microcavity thickness is chosen so that the light source, that is, the EZ, is centered at a destructive interference node, as in (c), so small shifts in the EZ position can result in clear shifts of the destructive interference resonance in the emission spectrum. The charge carrier energy level structure is shown in Figure S1, Supporting Information.

are thought to limit the performance of phosphorescent OLEDs and TADF OLEDs.[10,11] During OLED operation, the triplet–polaron interaction causes undesirable efficiency roll-off (i.e., increased quenching of excited states at higher current densities) and degradation (e.g., increasing the number of molecules with some of their intramolecular bonds irreversibly dissociated), resulting in less emitted light. Understanding and managing exciton dynamics is therefore of great significance in the design of modern TADF OLEDs.[12,13] These internal nanoscale processes are often difficult to observe, so there is

© 2022 The Authors. Advanced Materials published by Wiley-VCH GmbH

15214095, 2022, 29, Downloaded from https://onlinelibrary.wiley.com/doi/10.1002/adma.202201409 by EVIDENCE AID - BELGIUM, Wiley Online Library on [21/12/2022]. See the Terms and Conditions (https://onlinelibrary.wiley.com/terms-and-conditions) on Wiley Online Library for rules of use; OA articles are governed by the applicable Creative Commons License

substantial trial and error involved in the optimization of OLEDs. This is a labor, time, and material intensive process, which involves many deposition runs. Moreover, due to incomplete physical insight, learning outcomes for one stack may not be transferable to another.

Knowledge of the EZ in LEDs can give information on these internal processes. The EZ is the relative amount of light emitted from each position along the direction normal to the deposited layers. It is the convolution of the recombination, excited state diffusion, and quenching profiles. The importance of emission zone knowledge is due to the general features of multilayered OLED stacks; 1) energetic discontinuity at the layer interfaces and 2) spatially localized molecular wavefunctions. For OLEDs, energetically heterogeneous interfaces are necessary to confine positive and negative charges and to efficiently create excitons within the emission layer (EML). However, the confinement of charges could lead to a concentrated polaron density at one side of the EML and accordingly, the exciton formation would dominantly take place at the same side. Unlike in inorganic crystals, where the wavefunctions are delocalized anywhere, an exciton in an organic film is usually localized at an individual molecular site. The exciton diffusion length of a small molecular system is merely the size of a few molecules,[14,15] meaning that most excitons stay in the vicinity of the polaron concentration peak, so that the cross section of triplet–polaron collision is quite large. To avoid such radical interactions in terms of device optimization, it is crucially important to control the charge balance and to maintain a favorable emission zone distribution, guided by appropriate analyses. In modern (small molecule) OLEDs, the position of the EZ has been strongly linked to the external quantum efficiency (EQE) (via quenching at interfaces by accumulated charge carriers)[16–18] and the device lifetime.[19] Similarly, the EZ has been linked to the EQE roll-off and lifetime of PeLEDs[20] and QD LEDs.[21,22]

The EZ is difficult to measure because the EZ size is below the optical diffraction limit and therefore, standard LED emission spectra are not very sensitive to emission zone position. From Figure 1a, it can be seen that for an OLED with its microcavity optimized for maximum light outcoupling and EQE (standard or bright device type), the emission spectrum at 0° does not significantly change shape for the various individual infinitely thin emission zones shown in Figure 1b. Previously, sensing layers have been used to indirectly measure the EZ,[23,24] but the dyes of lower emission energy used in this method often act as charge traps, which change the device charge dynamics. Furthermore, many devices are needed for a single emission zone measurement, and therefore, meaningful results can only be extracted if the device-to-device repeatability is high.

To measure the location of the emission zone, a promising, destructive interference microcavity method[6,7] is known, which utilizes optical interference to reach superresolution, as also used in microscopy.[25] In this method, an LED microcavity formed by the two electrical contacts is fabricated, which gives destructive interference in the emission spectrum (dark device). This destructive interference is conventionally centered in the angular spectrum at ≈45°. The destructive interference pattern depends strongly on the position(s) of the different emission zones in the OLED microcavity. Therefore, emission

Table 1. Summary of properties of bright and dark devices.

Device type	Optical outcoupling	Sensitivity to emission zone	Emitters—highly reflective contact distance (this work: ETL thickness)
Bright	High	Low	Small
Dark	Low	High	Large

zone information can be obtained from an analysis of the emission spectra of such dark devices. In the conventional angular method, usually 10 angles from 0° to ≈90°, at a spacing of ≈10°, are measured.[26–28] The full angular range is measured to obtain the maximum emission zone information (see Discussion S1, Supporting Information which shows the angular behavior of bright and dark devices). For reference, the properties of bright and dark device types are summarized in **Table 1**.

However, only a few experimental results using the destructive interference microcavity method have been published for modern (small molecule emitter) OLEDs.[26–28] Mac Ciarnáin et al.[26] measured emission spectra of a phosphorescent OLED into air from 0° to 88° in steps of 4° and concluded that the emission zone was not confined to the EML or that it was concentrated at the EML interfaces. They stated an abnormally low internal quantum efficiency of around 30% (by definition, the internal quantum efficiency, in comparison with EQE, does not include optical outcoupling). Regnat et al. measured phosphorescent and TADF OLED emission spectra from 0° to 70° in steps of 10° using a cylindrical lens to extract additional light and the simulated emission spectra were fitted to the experimental by varying the EZ and intrinsic spectrum simultaneously.[27,28] The phosphorescent emitter study resulted in a U-shaped EZ and concluded that it can be a general feature of OLEDs.[27] The device efficiency was not reported. The proceeding study on a TADF exciplex host with a fluorescent emitter device also showed U-shaped EZs.[28] The physical explanation given for such an EZ was a build-up of charges at the interfaces. The device EQE here was given as ≈10%. Regarding modern (small molecule) OLEDs, to our knowledge, no study has been performed to measure the EZ trend with the device lifetime, or indeed to measure the EZ of a high efficiency device.

The few publications of such a promising method could be due to the method's complexity, in that it requires a measurement setup capable of precisely aligned, polarization-controlled detection of many angles. Also, there may be challenges due to device dynamics during the several minutes time required for a single emission zone measurement. Another complication of the method is that the emission zone results are for a dark device, with a thicker transport layer than the normal bright device, so the charge balance could be different in both cases. Care needs to be taken with the interpretation of such results. For these reasons, in this work, an alternative single emission spectrum measurement method and corresponding measurement methodology was developed with the aim to optimize OLED stacks.

Gather et al. first used an unpolarized 0° emission spectrum measurement and not emission from multiple angles to analyze the EZ of a single layer polymer OLED.[29] This was to avoid difficult and sometimes imprecise angular measurements.

© 2022 The Authors. Advanced Materials published by Wiley-VCH GmbH

15214095, 2022, 29, Downloaded from https://onlinelibrary.wiley.com/doi/10.1002/adma.202201409 by EVIDENCE AID - BELGIUM, Wiley Online Library on [21/12/2022]. See the Terms and Conditions (https://onlinelibrary.wiley.com/terms-and-conditions) on Wiley Online Library for rules of use; OA articles are governed by the applicable Creative Commons License

15214095, 2022, 29, Downloaded from https://onlinelibrary.wiley.com/doi/10.1002/adma.202201409 by EVIDENCE AID - BELGIUM, Wiley Online Library on [21/12/2022]. See the Terms and Conditions (https://onlinelibrary.wiley.com/terms-and-conditions) on Wiley Online Library for rules of use; OA articles are governed by the applicable Creative Commons License

A challenge of this approach for single layer devices is that the destructive interference resonance which contains the EZ information will not necessarily be visible at 0° emission. Depending on the EML thickness and the EZ, it may be centered at some other angle or not be visible at all. Modern OLEDs, PeLEDs, and QD LED stacks have transport layers. In this work, a technique is introduced where the transport layer thickness can be tuned to concentrate the microcavity destructive interference resonance into the 0° emission spectrum (Discussion S1, Supporting Information), which will be experimentally measured.

The principle of the adapted single emission spectrum method is outlined in Figure 1 and the technique itself is explained in the Experimental Section. It should also be noted that, in this work, it is not the angular behavior that is most important to understand the meaning of bright and dark devices. In the conventional angular emission zone measurement method, the angular variation is used to obtain emission zone information. In this work, we show that there is a way to distinguish all practical emission zone shapes from analyzing only a single angle (Figure S2, Supporting Information), which offers the multiple advantages outlined in the Experimental Section. In this single angle method, device dynamics during the less than 1 s measurement time should be a much lesser effect. We also use the angle of 0° for the specific advantage that almost every OLED research laboratory already performs such emission spectra measurements, so no additional measurement setup is required. To understand the meaning of bright and dark devices here, we must observe the sensitivity of each type of device to different emission zones at a single emission angle of 0°. This is what is compared in Figure 1a,c where the emission zones, shown in Figure 1b, are individual delta functions at different positions in the EML, to give the clearest example of the principle. A high sensitivity to different emission zones is given by dark devices, allowing us to measure the emission zone in the LED.

Furthermore, by using only a single angle, the single emission spectrum emission zone measurement method can allow observation of below second-timescale charge dynamics, for example, in perovskite LEDs[30,31] and can also be used for quantum dot LEDs. In Discussion S1.5, Supporting Information, a simulation of the method's ability to distinguish all practical emission zones for a common perovskite LED and quantum dot LED is presented. Experimental measurements of perovskite and quantum dot LED emission zones have not been shown in the literature. In this work, the method allows the current density, device structure, EZ, and lifetime relationships for an OLED to be comprehensively illustrated. Thereby, a tripled lifetime and efficiency, compared with the longest TADF OLED lifetime found in the literature[4] is demonstrated.

2. Results and Discussion

2.1. Procedure to Optimize LED Material Systems via Emission Zone Measurement

In this section, a procedure based on single-emission spectrum measurements, to obtain emission zone knowledge, is shown with the goal of optimizing a TADF OLED material system. First, in Section 2.2, the structure of dark devices is varied to see the effect on the EZ at a range of current densities. Then, in Section 2.3, the EZ relationship with device ageing in different current density regimes is examined to compare with the results of degradation studies in the literature. In Section 2.4, it is analyzed whether bright devices have the same EZ trends as were measured for the bright devices. The EZ relationship with bright device lifetimes is then examined. Finally, a high performance bright device is presented.

2.2. Emission Zone Relationship to Device Structure

In **Figure 2**, experimental 0° emission spectra (red curves in upper graph parts) of five D1 devices with five different emitter concentrations are shown at various current densities. Discrete Gaussian EZ functions (green bars in lower graph parts) are varied to give well-fitting simulated spectra (black curves in upper graph parts). See Figure S2, Supporting Information and Experimental Section for fitting details. Observing the trend in each column in Figure 2 and the current density–voltage (J–V) curves in **Figure 3**a, it appears that increasing the emitter concentration relatively increases the electron transport across the EML, as expected from the charge-transport energy level structure, where electron transport should occur mainly through the emitter, resulting in an electron accumulation at the EML–hole-blocking layer (HBL) interface when emitter concentration is low. A previous publication on this EML also assumed this to be the case.[5] With increasing current density along each row in Figure 2, the EML hole transport appears to relatively increase compared to the electron transport. For the lowest concentration of 1%, additional blue emission, most likely from the mCBP (3,3′-di(9H-carbazol-9-yl)-1,1′-biphenyl) EML host[32,33] instead, can be observed.

Electron-only device (EOD) and hole-only device (HOD) measurements have previously been performed for our mCBP:4CzIPN emission system.[5] Only the HBL material differed to those in our stack. Nonetheless, the measured highest occupied intrinsic orbital (HOMO) and lowest unoccupied intrinsic orbital (LUMO) of both HBLs are practically the same. This study revealed that varying the 4CzIPN emitter concentration changed the n-type currents, while this same variation did not influence the p-type currents. These results clearly indicate that 4CzIPN is the electron transporter in the system and mCBP is the hole transporter. Note that OLED stacks were prepared with different ETLs (devices B1 and D1 with BPy-TP2, and B2 and D2 with SF3-TRZ:Liq, see Figure 1d). The zero-field SCLC electron mobility of spirobifluorene-triazine is on the order of 10^{-5} cm^2 V^{-1} s^{-1}.[35] A superior electron mobility of BPy-TP2 was postulated by the steep SCLC slope of the EOD J–V curve,[36] and we indeed confirmed the superiority of BPy-TP2 electron transport to SF3-TRZ:Liq by comparison of their device J–V curves (Figure S3, Supporting Information). Nevertheless, the EZ trends of devices D2 with BPy-TP2 ETL (Figure S4, Supporting Information) are nearly identical to those of devices D1 with the SF3-TRZ:Liq ETL (Figure 2) with respect to variation of emitter concentration. This implies that the n-/p-type current balance in the device is insensitive to the

 © 2022 The Authors. Advanced Materials published by Wiley-VCH GmbH

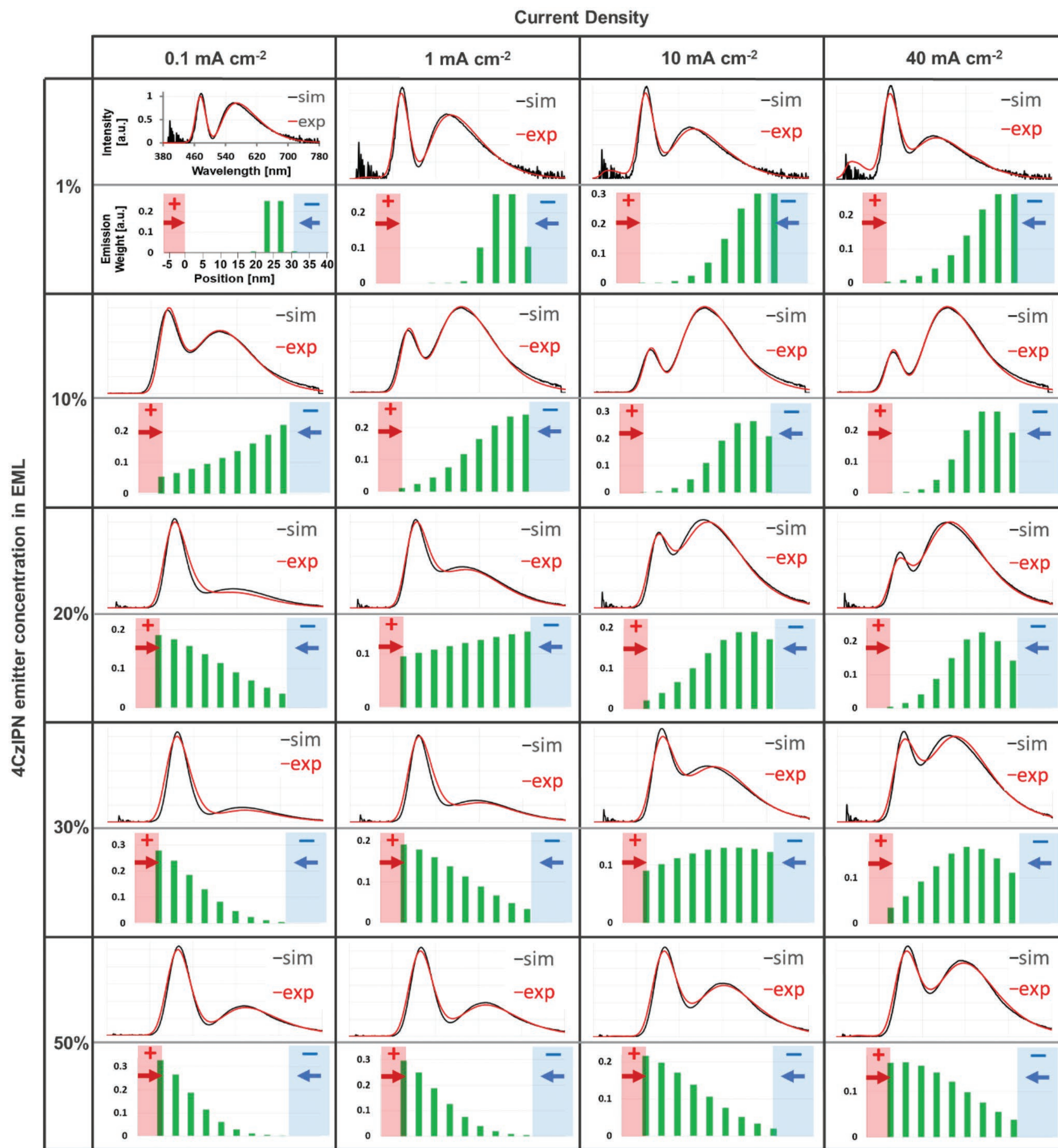

Figure 2. Fitted EZs for device D1 are shown. The axes for 1% with 0.1 mA cm^{-2} are the same for all other graphs, except that the emission weight magnitudes vary due to EZ area normalization. Above graphs of each table entry show measured (red) and simulated (black) 0° emission spectra. Simulated curves are noisy due to using an experimentally extracted intrinsic spectrum. Below graphs show the EZ as weighted emission source positions in the EML (green bars) which give the simulated spectrum above. The simulated spectra are fitted to the experimental while varying only the EZ as a discretized Gaussian function (see Experimental Section for further details). Each row represents a single device. All simulated spectra in the figure have the same microcavity thicknesses as device thickness uniformity < 1 nm (see Experimental Section). Spectral changes in a row are caused only by a varying EZ with current density. Spectral changes along columns are due to the EZ changing with emitter concentration and to a lesser degree, concentration-quenching shifted[34] intrinsic spectra (Figure 3b), which are independently extracted from bright devices and accounted for in each simulation.

difference in ETL mobility. Also, no large EZ shift or lifetime changes are observed for a hole-transport-layer thickness variation from 15 to 120 nm, for both ETLs (Figures S5,S6, Supporting Information). The high repeatability of the method is illustrated by such closely matching emission zone results from different deposition runs.

 © 2022 The Authors. Advanced Materials published by Wiley-VCH GmbH

15214095, 2022, 29, Downloaded from https://onlinelibrary.wiley.com/doi/10.1002/adma.202201409 by EVIDENCE AID - BELGIUM, Wiley Online Library on [21/12/2022]. See the Terms and Conditions (https://onlinelibrary.wiley.com/terms-and-conditions) on Wiley Online Library for rules of use; OA articles are governed by the applicable Creative Commons License

15214095, 2022, 29, Downloaded from https://onlinelibrary.wiley.com/doi/10.1002/adma.202201409 by EVIDENCE AID - BELGIUM, Wiley Online Library on [21/12/2022]. See the Terms and Conditions (https://onlinelibrary.wiley.com/terms-and-conditions) on Wiley Online Library for rules of use; OA articles are governed by the applicable Creative Commons License

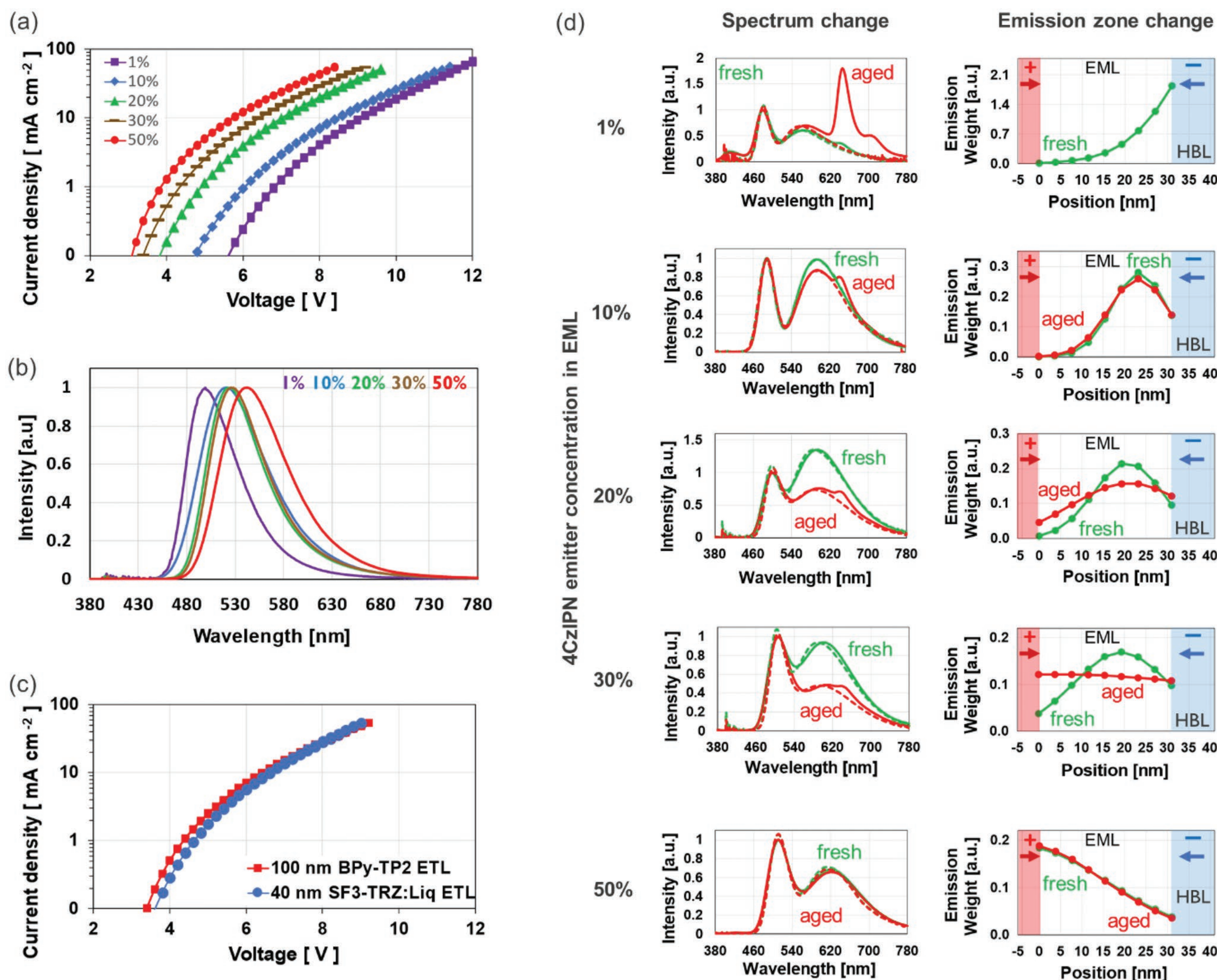

Figure 3. a) J–V curves for D1 devices with varying emitter concentration. b) Intrinsic spectra extracted from B1 devices with varying emitter concentration. c) 30% emitter concentration device B2 and D1 having overlapping J–V curves. d) Left: Fresh (green curves) and aged (40 mA cm^{-2} constant current to 50% radiance, shown as red curves) spectra of the D1 devices, experimental curves are solid lines and simulated curves dashed. Right: Fitted fresh (green curves) and aged (red curves) EZs of the spectra are shown. EZ changes cannot be calculated for 1% devices as the level of HBL emission[33] is too high. These spectra are slightly different than in Figure 2 because different devices with different substrate radial position in the same deposition run, characterized to have slightly different thicknesses must be used for each lifetime measurement at each different current density.

These results outline an important aspect in the optimization of this stack, that the conductivity of the transport layers, which is a function of mobility and electric field (related to thickness) does change the operational voltage but does not significantly change the n-/p-type current balance in the EML because current density in a device is uniform everywhere. The EZ peak is the position where electrons and holes can most efficiently meet, but it is also the position where many polarons (which do not contribute to the recombination current) are waiting for their counterparts and/or interaction with excitons. It is concluded that the electron injection into the EML is the charge-transport constraint of this system, even if the transport layers are changed. Accordingly, in this stack, the EZ can be sensitively controlled by adjusting the emitter concentration.

2.3. Emission Zone Relationship with Device Ageing

Next, the EZ relationship with device ageing was investigated by measuring the lifetime of devices with the various emitter concentrations and ETLs and by also comparing emission spectra before and after ageing. Lifetime data were measured for all device stacks at three different constant current densities: 1, 10, and 40 mA cm^{-2} and is shown in **Figure 4**. Only one lifetime measurement at a single current density can be performed on an individual device, so multiple devices from the same sample are used to measure lifetimes at the other current densities. Actual data were measured for all current densities; the accelerated ageing assumption was not used as it was proved invalid for devices where the EZs change with current density.[37]

© 2022 The Authors. Advanced Materials published by Wiley-VCH GmbH

15214095, 2022, 29, Downloaded from https://onlinelibrary.wiley.com/doi/10.1002/adma.202201409 by EVIDENCE AID - BELGIUM, Wiley Online Library on [21/12/2022]. See the Terms and Conditions (https://onlinelibrary.wiley.com/terms-and-conditions) on Wiley Online Library for rules of use; OA articles are governed by the applicable Creative Commons License

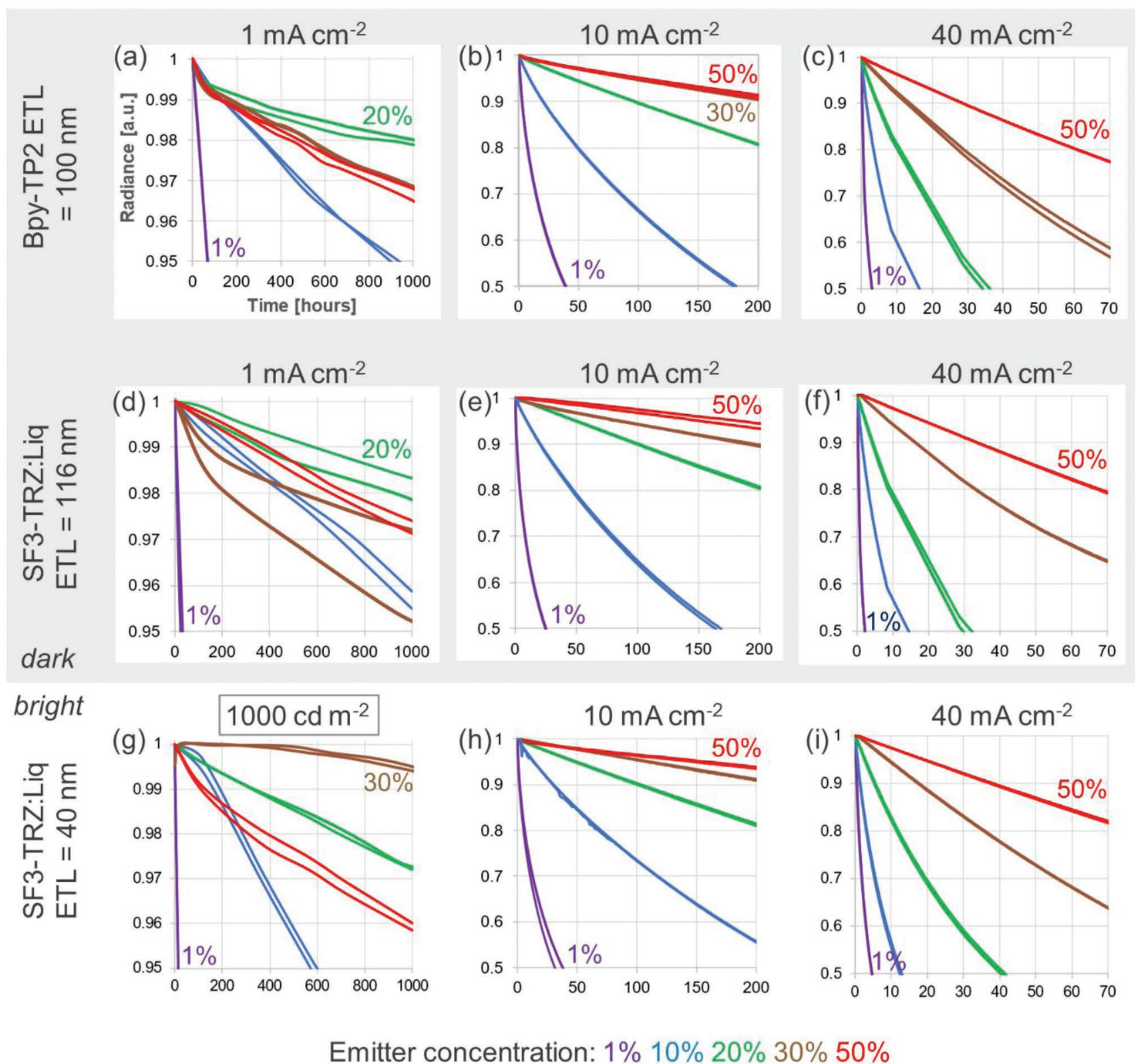

Figure 4. The axis titles in the upper left graph are the same for all other graphs. The three graph rows represent devices with three different ETLs. Measurements for dark devices are shown above in the top two rows in the grey box and bright devices in the bottom row. The specified current density ageing condition is labeled on the top of each graph. Bright devices are measured at an initial luminance of 1000 cd m^{-2} (between 1.55 and 2.15 mA cm^{-2}) instead of 1 mA cm^{-2} as is common for display applications. The colored legend at the bottom of the figure shows the emitter concentrations. Two devices were measured and are shown for each measurement to show device repeatability.

2.3.1. Ageing at 10 and 40 mA cm^{-2}

It appears that the same degradation mechanism dominates at current densities of 10 and 40 mA cm^{-2}, as the same lifetime trend is observed—the device lifetime increases with emitter concentration for both bright and dark device ETLs. This correlates with dark device EZs being less concentrated at the HBL interface in Figure 2. Bright device EZs cannot be directly measured (see Figure 1), however, the lifetime trend is the same as for the dark devices, which suggests that they have comparable EZs. Additionally, EZs were not measured to significantly change, for dark devices with different ETLs. At low current density, (Figure 4a,d,g), degradation appears to proceed differently. This regime will be discussed in a later section.

Next, in Figure 3d, the 40 mA cm^{-2} dark device D1 spectra (comparison with D2 devices in Figure S8, Supporting Information) are compared before and after constant current ageing to 50% radiance. An additional red emission peak at 640 nm can be observed. This is clear emission from the 2,4-diphenyl-6-(9,9′-spirobi[9H-fluoren]-3-yl)-1,3,5-triazine (SF3-TRZ) HBL under electrical operation as well studied by Tanaka et al.[33] They postulate that when more holes enter the HBL (which can

 © 2022 The Authors. Advanced Materials published by Wiley-VCH GmbH

15214095, 2022, 29, Downloaded from https://onlinelibrary.wiley.com/doi/10.1002/adma.202201409 by EVIDENCE AID - BELGIUM, Wiley Online Library on [21/12/2022]. See the Terms and Conditions (https://onlinelibrary.wiley.com/terms-and-conditions) on Wiley Online Library for rules of use; OA articles are governed by the applicable Creative Commons License

be tracked here with the EZ), anion and cation SF3-TRZ species form under electrical operation and recombination occurs resulting in red emission.[38] This emission process coincided with an irreversible degradation of the SF3-TRZ, as observed from a lowering of the current with time in the same device structure of this work but without the EML.[33] Similar spectral changes with ageing at 10 mA cm^{-2} are shown in Figure S9, Supporting Information. In Figure 3d, the additional red peak is largest for the 1% device where most holes should enter the HBL and smallest for 50% where the least holes should enter the HBL. That the HBL emission trend matches the measured EZs is also independent evidence for the fidelity of the single emission spectrum EZ measurement method. EZ changes are also shown on the right of Figure 3d. After ageing, the EZs at 10%, 20%, and 30% are observed to become less concentrated at the HBL interface. A consideration of possible intrinsic spectrum changes with ageing is given in Discussion S3, Supporting Information.

2.3.2. Comparing the 10 and 40 mA cm^{-2} Optical Results with the Degradation Literature

In the literature, degradation mechanisms have been studied for the same EML of this work at 15% or 20% doping concentration: At 3 mA cm^{-2} current density, the host mCBP excited state, not the 4CzIPN emitter, was found to be very unstable.[39] In Figure 2, EML hole transport dominates even more at current densities higher than 3 mA cm^{-2} so this mechanism can represent our 10 and 40 mA cm^{-2} ageing. Sandanayaka et al. analyzed EODs and HODs featuring our EML, from 0 to 3000 mA cm^{-2} and also found no degradation of the 4CzIPN emitter. They also observed that injected electrons do not affect excitons, but injected holes do. mCBP and 4CzIPN positive cations were found to quench excitons due to their absorption spectrum overlap with the emitter but no overlap was observed for the negative anions.[40] Tanaka et al. found, over the same current density range of our work, that the main device degradation mechanism was triplet polaron interactions from excess holes reaching the (SF3-TRZ) HBL resulting in quenching and non-radiative center formation.[6] Yamaguchi et al. concluded that the main degradation mechanism was the presence of exciton quenchers generated by HBL degradation products.[41] For a blue emitter system, a decrease in hole mobility with degradation of the mCBP host was found, probably due to hole trap formation.[42]

A hypothesis that agrees with the optical results of this work and the degradation literature is that lower emitter concentration EMLs result in more holes crossing the EML and reaching the HBL interface (Figure 2). This results in more HBL emission (Figure 3d) and HBL degradation.[33] With ageing, this hole-dominated current in the EML (for lower emitter concentrations) degrades the unstable host more than the emitter, leading to an EML charge balance shift to the anode side. This host degradation seems to have a larger effect on the EML charge balance than the HBL degradation, agreeing with the EZ-device structure findings earlier, where the EML, not the transport layer composition is dominantly responsible for the EML charge balance. The observed EZ change could also be caused by localized exciton quenching; emission close to the HBL interface could be deactivated by exciton-polaron interactions due to the interfacial electron accumulation and/or the HBL degradation products.

In summary, at the higher current densities of 10 and 40 mA cm^{-2}, the device lifetime increases proportionally with emitter concentration and the EZ-center distance from the HBL. There is also increasing HBL emission for EZs closer to the HBL. With increasing ageing, increasing emission is observed from the (SF3-TRZ) HBL, which should be associated with device degradation.[33] However, additionally, since the device lifetime increases proportionally with emitter concentration, there could be a significant lifetime extension contribution of an increasing proportion of excitons being formed on the emitter instead of the more instable mCBP host. From evidence in this work, we conclude that, for higher current densities, the EZ is likely to be a significant factor for ageing, but the proportion of exciton formation on 4CZIPN could also be a significant factor. Further work can address this if well performing mixed host materials are found for this emitter. The term “mixed hosts” refers to two hosts co-doped with the emitter in the EML, one which is electron transporting and one hole transporting. Then the EZ could be controlled without changing the emitter concentration.

2.3.3. Ageing at 1 mA cm^{-2}

At 1 mA cm^{-2} current density, D1 and D2 device lifetimes follow the same order up to 20% emitter concentration. However, the 30% and 50% devices show a lower lifetime, relatively, than in the higher current density trend. Using Figure 2, this can be explained by degradation processes when the EZ is concentrated at the electron-blocking layer interface, being comparable to those where the EZ is concentrated at the HBL interface. The lifetime is longest for the most balanced EZ where the emission is least concentrated at the interfaces, where charges can build up, as predicted in the literature.[16–19] No remarkable EZ shift is observed at 1 mA cm^{-2} as there is not much radiance reduction after 1000 h driving (Figure S13, Supporting Information) indicating little EML material degradation, agreeing with the long lifetimes measured at around 1 mA cm^{-2} current density. In summary, at the lower current densities of around 1 mA cm^{-2}, the lifetime trend cannot be explained by the proportion of excitons formed on the more stable emitter alone as the highest emitter concentration does not result in the best lifetime. However, the lifetime increase can be explained by a more balanced EZ. Additionally in this low current density region, we calculate a charge balance efficiency (CBE) of 96%, (see Section 2.4) meaning that there should not be a lot of excess polarons for degradation phenomena to occur. This leads to the hypothesis that the measured balanced EZ is the main reason for the ultralong device lifetime, at this low current density relevant to display applications.

2.4. Lifetime Trend in Bright Devices

In this section the focus is to try to explain the lifetime trend for efficient bright devices, which are relevant for display

© 2022 The Authors. Advanced Materials published by Wiley-VCH GmbH

15214095, 2022, 29, Downloaded from https://onlinelibrary.wiley.com/doi/10.1002/adma.202201409 by EVIDENCE AID - BELGIUM, Wiley Online Library on [21/12/2022]. See the Terms and Conditions (https://onlinelibrary.wiley.com/terms-and-conditions) on Wiley Online Library for rules of use; OA articles are governed by the applicable Creative Commons License

applications. An issue with the destructive interference microcavity method for EZ measurement is that the EZ results are for dark devices. Dark devices are not useful for applications due to their very low outcoupling efficiency due to the induced destructive interference in the emission. In this work dark devices are used only as EZ sensing devices. The goal is to fabricate long lifetime bright devices and try to understand the lifetime trends to guide future device optimization.

Dark devices have, in the case of this stack, a thicker ETL than the bright devices. Both these devices could therefore have different charge balance and EZs. In Section 2.2, it was discussed that the EZs did not change significantly with the different ETL-material dark devices even though they had significantly different *J*–*V* curves. So, it seems that the ETL should not strongly affect the EZs, for this stack. Nonetheless, in this work, as an added step, we have introduced the engineering of the thin transport layer for the bright device to have an overlapping *J*–*V* curve with the thick transport layer dark device (Figure 3c). The SF3-TRZ:Liq ETL material was chosen for these bright devices so that the dark and bright devices would have overlapping *J*–*V* curves and also due to its better performance (Figure S10, Supporting Information).Then as a first approximation, it was assumed that these bright and dark devices have closely matching EZs.

We now compare the lifetime and EZ trends. At the higher 10 and 40 mA cm^{-2} current densities the bright and dark device lifetime trends match. This could be because they have closely matching EZs and the lifetime trend is dominantly controlled by the EZ, or that the lifetime trend is dominantly controlled by the proportion of exciton formation on the more stable emitter molecule.

The main goal of this work was to fabricate long lifetime bright devices at the low current density region of interest to give a standard luminance of 1000 cd m^{-2} for display applications. At low current densities, the bright and dark device lifetime trends again match except that the 30% emitter bright device lifetime (Figure 4g) is longer than for the 30% emitter dark device (Figure 4a,d). However, the actual current density is not exactly the same for the measured dark and bright lifetimes, so the EZs will be different. At the higher current density (1000 cd m^{-2}) used for the bright device lifetime measurement (1.7 mA cm^{-2}), the 30% EZ becomes relatively more balanced (Figure S14, Supporting Information). This could explain the improved lifetime for the 30% emitter bright device compared to the 20% emitter dark device. The literature generally predicts[16–19] that the lifetime will be longest for the most balanced EZ.

The longest published lifetime for a TADF OLED found in the literature is T_{95} = 1315 h with an EQE = 6.2% which was measured at 1000 cd m^{-2}.[4] In that work, the lifetime was most probably extended (the triplet–polaron interaction reduced) by simultaneously sacrificing EQE via the introduced Liq quenching layer. In this work, that performance is tripled, resulting in a T_{95} lifetime at 1000 cd m^{-2} of 4500 h with an EQE of 20% (**Figure 5**). The electroluminescence spectrum and CIE color coordinates of this device are shown in Figure S15, Supporting Information. A high emitter doping of 30% is used to relatively increase the electron transport in the EML and balance the EZ, which correlated with a longer device lifetime. OLEDs with such a high emitter concentration have not been studied much due to concentration quenching concerns. However, the measured photoluminescence quantum yield (PLQY) of 77% for our EML does not change when increasing the concentration from 20% to 30% (Figure S16, Supporting Information). We can have a high EQE for our optimized device even though we have a very high emitter concentration because the PLQY remains high. This suggests that concentration quenching is not such a strong effect for this emitter system. The CBE was calculated according to[43]

$$\mathrm{EQE} \approx \eta_{\mathrm{S/T}} \times \mathrm{PLQY} \times \mathrm{CBE} \times \mathrm{Outcoupling} \tag{1}$$

where $\eta_{S/T}$ represents the singlet triplet ratio (the fraction of excitations that luminesce with regard to spin statistics) which ≈1 for TADF systems. The optical outcoupling efficiency for this device was calculated using the Setfos software to be 0.27 (see Experimental Section). This resulted in a CBE for this optimized OLED of 96%, which agrees with the balanced EZ measurement result. If the CBE was 100%, then the resulting device EQE would be 20.8%.

In summary, for 1000 cd m^{-2} driving condition, we have observed a correlation of a more balanced EZ with a longer device lifetime, as predicted in the literature. Additionally, we calculate a 96% CBE, which should mean that less excess

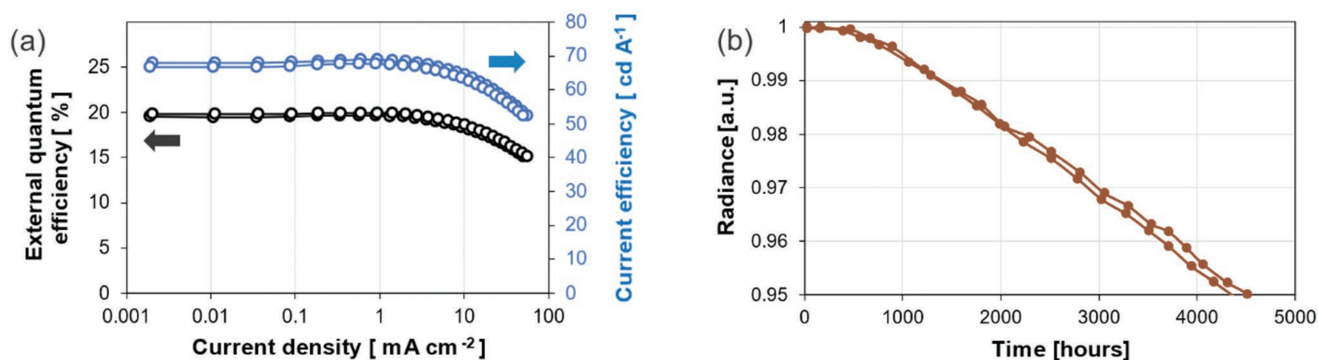

Figure 5. Results for the 30% emitter concentration device B2 with the SF3-TRZ:Liq ETL are shown. a) EQE and current efficiency and b) 1000 cd m^{-2} constant current lifetime. Two devices were measured and are shown to illustrate device repeatability. The electroluminescence spectrum, CIE color coordinates, and *J*–*V*–luminance plots for this device are shown in Figure S15, Supporting Information.

 © 2022 The Authors. Advanced Materials published by Wiley-VCH GmbH

ADVANCED MATERIALS
www.advmat.de

polarons are present for degradation effects to occur, decreasing the lifetime. We have found, from studying the evidence, that a more balanced EZ is the most probable reason for the longer device lifetime.

3. Conclusion

In this work, the performance of the best thermally activated delayed fluorescence organic LED lifetime found in the literature was tripled with a T_{95} lifetime at 1000 cd m^{-2} of 4500 h with an EQE of 20%. A procedure was shown to optimize an LED stack, by tracking the emission zone. The emission zone relationships to device structure, current density, device lifetime, and ageing were visualized for the first time. Tracking of the varying emission zones with doping concentration and current density allowed for the emission zone balance to be controlled. For this material system, the emission zone balance was found to be dominantly regulated by the charge-transport properties of the EML itself. The constraint of the OLED system studied was identified as the electron injection/transport in the EML. A high emitter concentration of 30% allowed for the most balanced emission zone which correlated with the longest device lifetime. If found for this emitter, a well-performing mixed host could enable a lower emitter concentration and lower concentration quenching and therefore, a higher efficiency.

At 10 and 40 mA cm^{-2} current densities, the emission zone was correlated with the device lifetime, but the higher proportion of exciton formation being on the more stable emitter could also be responsible for the higher lifetime. At low current densities around 1 mA cm^{-2}, the lifetime trend cannot be explained by the emitter proportion effect, as the highest emitter concentration does not result in the best lifetime. The measured, more balanced emission zone can explain the increased lifetime (as also predicted by the literature) which agrees with the 96% CBE calculated for the ultralong lifetime device.

To achieve this experimental insight, an adapted measurement method was used. Where previously, a complex optical measurement system was needed, the introduced single emission spectrum method is accessible in every optical lab. The only measurements required are the 0° emission spectrum using no additional polarization or outcoupling optics. This data are generally already measured for all LEDs in research and development. Therefore, no additional measurement or setup is necessary. The single emission spectrum method allows sub-second emission zone measurement resolution, compared to the several minutes resolution of the conventional angular method. This is important to minimize systematic errors when measuring devices with significant charge dynamics during the measurement time. Additionally, a method to obtain actual device microcavity thicknesses by fitting only the device emission spectra without using ellipsometry and which gives a thickness accuracy of <1 nm is established (Figure S19, Supporting Information).

This accessible method allows the distinguishing of all practical emission zones at all luminescing current densities. An experimental measurement of the emission zone is given which does not require knowledge of multiple electrical parameters which are difficult to accurately know for a real device. It is only necessary to characterize the device layer thicknesses, optical constants, and 0° emission spectra. Although the method has been applied to a green OLED in this work, the method should be applicable to any LED emission spectra. This is because, in the method an arbitrary intrinsic spectrum is extracted and then convoluted with a simulated microcavity effect based on the position of the emitters, and then compared with the arbitrary experimental emission spectrum. This method can be used to give valuable insight into the internal processes in LED stacks, which can accelerate their development.

4. Experimental Section

Single-Emission Spectrum Measurement Technique: For measuring LED emission zones, an adapted, single emission spectrum method with advantages over the conventional angular method[26–28] was introduced here. The main concept was that the transport layer thickness could be tuned to concentrate the microcavity destructive interference resonance into the 0° emission spectrum. The principle of this method is illustrated in Figure 1c. It could be seen that a dark OLED with its microcavity thickness set to give a destructive interference pattern in the emission spectrum, was very sensitive to the emission position (the different individual delta function emission zones are defined in Figure 1b). In this way, such a destructive interference microcavity could give emission zone position information to nm accuracy order (see resolution discussion in Experimental Section). Even though only one angle was measured, one could obtain sufficient resolution to distinguish all practical EZs (see Discussion S1, Supporting Information for a comparison of the sensitivity of the methods). This was possible as the destructive interference resonance was strongest at a single angle, then got weaker at further away angles. The visualization of the EZ enabled the understanding to then engineer an optimized EZ device.

Device Fabrication: Computer-controlled[44] thermal evaporation of the OLED materials was performed as described in the literature[11] resulting in 1 nm repeatability of microcavity thicknesses (see later section) and high repeatability of lifetimes.[44] Regarding the stack layer thicknesses, all thicknesses were taken from an established stack in the literature.[5] Devices were deposited under low water pressure of 10^{-7} Pa.[45] Masks enabled separate deposition onto the four quarters of the substrate, for each layer deposition stage, allowing four separate-structure devices per deposition run.

Optical Simulation: The transfer-matrix method was used to model the propagation of electromagnetic waves through the multilayer LED stack. In this work, Setfos commercial software version 5.0 from Fluxim AG[46] was used. A mathematical treatment of the transfer-matrix method as applied to OLEDs could be found in the literature.[6–8]

Additionally, in Setfos, the mode analysis setting was used to simulate the outcoupling efficiency of the optimized device of Section 2.4. It should be noted that OLED optical outcoupling depended on the average orientation of the emitter dipoles in the EML layer. In the literature, 4CzIPN doped in mCBP:B2PYMPM(1:1) was measured to have a slightly horizontal average emitter orientation (perpendicular component = 0.27, with 0.33 representing the isotropic case).[47] This value was used for the EQE calculation in Section 2.4. Using the 30% emitter internal spectrum from Figure 3b and the EZ for 30% emitter concentration at 1 mA cm^{-2} current density as could be observed in Figure 2, the outcoupling was calculated as = 0.27.

Microcavity Sensitive to EZ in Angular Range or at Single Angle: Gather et al. used an unpolarized 0° emission spectrum measurement and not emission from multiple angles to analyze the EZ of a single layer polymer OLED.[29] This was to avoid difficult and sometimes imprecise angular measurements. Additionally, with the conventional angular method,[26–28] there may be challenges due to device dynamics during the measurement time for a single emission zone. At low current densities, the measurement time for each emission zone at each current

© 2022 The Authors. Advanced Materials published by Wiley-VCH GmbH

15214095, 2022, 29, Downloaded from https://onlinelibrary.wiley.com/doi/10.1002/adma.202201409 by EVIDENCE AID - BELGIUM, Wiley Online Library on [21/12/2022]. See the Terms and Conditions (https://onlinelibrary.wiley.com/terms-and-conditions) on Wiley Online Library for rules of use; OA articles are governed by the applicable Creative Commons License

15214095, 2022, 29, Downloaded from https://onlinelibrary.wiley.com/doi/10.1002/adma.202201409 by EVIDENCE AID - BELGIUM, Wiley Online Library on [21/12/2022]. See the Terms and Conditions (https://onlinelibrary.wiley.com/terms-and-conditions) on Wiley Online Library for rules of use; OA articles are governed by the applicable Creative Commons License

density could take up to 10 min. At high current densities, the device state may change while measuring the ≈10 different angles. For these reasons, EZ measurements across the complete luminescing current density range of a device had not been measured before. Furthermore, optical anisotropy and the emitter orientation (ratio of parallel to perpendicular dipole emission components of emitter ensemble) of the involved materials could be neglected because only electromagnetic fields parallel to the device layers were significant in 0° emission into air.[48] A challenge of this approach for single layer devices was that the destructive interference resonance which contained the EZ information will not necessarily be visible at 0° emission. Depending on the EML thickness and the EZ, it may be centered at some other angle or not be visible at all. Modern OLEDs, PeLEDs, and QD LED stacks had transport layers. In this work, a technique was introduced where the transport layer thickness could be tuned to concentrate the microcavity destructive interference resonance into the 0° emission spectrum, which will be experimentally measured. The resonance contained the EZ information, as described in Figure 1.

Tuning a Microcavity to be Sensitive to EZ Information: First, a simulation must be performed to design a microcavity with the correct thicknesses to place the resonance in the 0° emission spectrum. As can be seen from Equation (2) below, to simulate the emission spectrum, a knowledge of certain optical functions was necessary. An accurate knowledge of the layer optical constants (n&k), the intrinsic spectrum, and the main microcavity thicknesses was required to have an accurate emission spectrum simulation. These functions were independently determined as explained in the following sections. Changing the light source (e.g., the EZ) distance to the highly reflecting contact changed the angle that the resonance appeared in, due to the geometry of the microcavity interference conditions. The outcoupling contact was less reflective, so it had a significantly lower effect on the microcavity interference. In the case of this work, the ETL was varied, as it effectively controlled the light source distance to the highly reflecting contact. Considerations on the electrical effect of changing the ETL thickness are found in the next section. It should also be noted that the position of the resonance strongly depended on the light source position, that is, the EZ, which may not yet be known. Therefore, a solution was to choose an ETL thickness which had destructive interference in the 0° emission spectrum for the simulations of all practical EZs, allowing them to be distinguished (as in Figure S2, Supporting Information). When the EZ was extracted, further iterations of the ETL thickness could be deposited to ensure maximum sensitivity to the actual EZ. Note that the EZ could change with current density, so further iterations could also take this into account to obtain the most sensitivity on the central current density in the range of interest.

Current Density–Voltage Behavior of Dark and Bright Devices: A disadvantage of the conventional microcavity EZ measurement method was that dark devices which were sensitive to the EZ had thicker transport layers than bright devices and so the different devices may have different charge balance and EZs. Different transport layer materials and doping concentrations (see electron-transport layer compositions in Figure 1d) were used in this work to have bright and dark devices having overlapping current density–voltage curves (Figure 3c). Comparing the lifetime trends with emitter doping concentrations for both bright and dark devices was also introduced in this work as a useful test of whether bright and dark devices had comparable EZs.

Deposited Layer Optical Constant Determination: Layer optical constants for the simulation were obtained from samples on a silicon substrate with an n,k spectrometer (n&k Technologies 1280 Broadband UV–vis Spectrometer) at near-normal reflectance angle to the layer. Samples with the same thickness as the target layer in the real stack were deposited on a 3 nm thick film of the previous layer in the real stack to have the layer growth conditions as close as possible to those in the real stack.

Intrinsic Spectra Extraction: Intrinsic spectra for each emitter concentration were independently extracted from bright devices where the EZ only slightly affected the emission spectrum shape (Figure 1a). In this way, knowledge of the EZ was not necessary to accurately obtain the intrinsic spectrum. To get the bright device intrinsic spectrum, the experimental emission spectrum of a bright OLED was divided by this simulated emission spectrum featuring a constant intrinsic spectrum (intrinsic spectrum magnitude equal to 1 at all wavelengths). See Equation (3) below and Figure S7, Supporting Information. This division was done in Microsoft Excel, which was well suited for matrix operations. The simulated emission spectrum was obtained from the Setfos software and was the sum of the microcavity modulation from each different EML position, using an arbitrary, for example, constant EZ, (multiplied by a constant intrinsic spectrum). This was performed for devices of each emitter concentration. The input EZ (Figure 1) and microcavity thickness had little effect on the intrinsic spectrum extraction when these bright devices were used. As mentioned before, when knowledge of the EZ was later obtained, an iterative approach could be used to reduce this small effect. It should be noted that the intrinsic spectrum could change slightly with current density. In this case, it should be measured at all relevant current densities. The assumption that the dark device intrinsic spectrum will be the same as the bright device was then used for fitting of the EZs from dark devices. This assumption should be valid as first, the EMLs were the same. Second, the transport layers did change but they were chosen so that the current–voltage behavior did not significantly change (see Figure 3c) and third, evidence was given in this article that the dark and bright device EZs should also not be different. This assumption seemed to work well in practice as the bright intrinsic spectra fit well when used to simulate the dark device spectra well in Figure 2. Care should be taken to control these factors so that the assumption could be justifiably used.

Actual Device Microcavity Thickness Evaluation: Uncertainty in the microcavity thicknesses was directly related to uncertainty in the extracted EZ position (Figure S17, Supporting Information). If, in the simulation, the emitter-cathode distance was incorrect, then the center of the fitted emission zone will shift position to compensate, so that the emitter–cathode distance was correct to fit the experimental spectrum, resulting in an error in the actual emission zone center position. Also, a 10% thickness deviation regarding detuning could lose EZ sensitivity (Figure S18, Supporting Information). Therefore, for dark OLEDs used for EZ analysis, the microcavity thickness needed to be known to an uncertainty of 1 nm. Ellipsometry required separate samples to be prepared and these may not accurately represent the actual device thickness. For example, where a rotating substrate was used during deposition, ellipsometry samples may have a different thickness than the actual device if the substrate radius was not the same. A procedure is outlined in Figure S19, Supporting Information to fit the microcavity thicknesses with an accuracy of <1 nm using only the device emission spectra, so the thicknesses were measured for actual complete devices. One of the four substrate quarters featured a thin 6 nm EML dark device which should be well modeled with a constant EZ due to exciton diffusion.[14,15] A constant EZ removed the EZ as a variable in the emission spectrum simulation, leaving only the microcavity thicknesses as variables in the emission spectrum fitting procedure. Dark devices were used as bright device emission spectra were not sensitive to microcavity thicknesses. Then, the same EML–cathode thickness was deposited for all four quarters. Finally, the only unknowns (apart from the intrinsic spectra, which were independently extracted from bright devices) when simulating the emission spectra of the 6 nm EML device would be the anode–source and source–cathode distance and the EML width which had different emission features and so could all be well extracted from fitting with the experimental spectrum. If the layer optical constants were close in value, individual layer thicknesses should not have a significant effect on the emission spectrum compared to the three “microcavity” thicknesses (Figure S19, Supporting Information). This method could also be used for a “fine tuning” tooling characterization of the deposition system to deposit target thicknesses accurately. Using these microcavity thicknesses, the only unknown (apart from the intrinsic spectrum, which was independently extracted before) in simulating the emission spectra of the other three devices with the real EML thickness of 31 nm, was the EZ. The other three substrate quarters could then have different emitter concentrations, for example, resulting, in this work, in various EZs and emission spectrum shapes from devices with a single microcavity

© 2022 The Authors. Advanced Materials published by Wiley-VCH GmbH

ADVANCED MATERIALS
www.advmat.de

thickness. The EZs could then be directly compared knowing that ETL thickness variation was not significant. Using such a simultaneous equation approach enabled a more accurate EZ fitting, together with the thicknesses fitted with the 6 nm EML device. In Figure 2, for example, the top three rows were from a single deposition where only the emitter concentration was varied using a shutter to deposit the different EMLs of the four devices in the deposition run one at a time. The bottom three rows were from another deposition where the microcavity thickness was verified to be the same thickness within 1 nm. The thin EML devices had not been studied for ageing due to their lower lifetimes than the standard thickness EML devices, most probably due to the increased charge accumulation in a smaller volume which should occur with such thin EMLs.

EZ as a Variable in a Linear Equation: In the conventional angular method,[7,26–28] both the unknown parameters, the intrinsic spectrum and the EZ were fitted simultaneously in a single linear equation which could result in errors (Figure S20, Supporting Information). The simplified linear equation for LED emission can be written,[8]

$$I_{\lambda_j,\theta_i} = \sum_{m=1}^{N} A_{\lambda_j,\theta_i}(z_m) \times M_{\lambda_j} \times p(z_m) \times \Delta z \tag{2}$$

where I is the far field intensity depending on the wavelength λ_j and θ_i is the observation angle to the stack normal. A is the energy emission density depending on the emitter position along the layer interface normal z_m, and M_{λ_j} is the intrinsic spectrum. $p(z_m)$ is the profile of the EZ which gives the weights of emission at each position and Δz is the EZ position step size. A graphic representation is shown in Figure S21, Supporting Information to aid understanding.

In this work, the intrinsic emission spectrum was separately obtained from an optimized outcoupling device where the EZ impact was negligible as suggested in a publication,[6] and the intrinsic spectrum was the only unknown, (graphic representation shown in Figure S7, Supporting Information)

$$I_{\lambda_j,\theta_i} = \sum_{m=1}^{N} A_{\lambda_j,\theta_i}(z_m) \times M_{\lambda_j} \tag{3}$$

allowing one to have the EZ as the single unknown fitting parameter in the linear equation.

EZ Fitting: The emission zone was fitted by comparing the experimentally measured with the simulated 0° emission spectrum. To simulate the emission spectra, the microcavity modulation from the different EML positions was calculated and each was multiplied by an individual weight. The emission from each position was then multiplied by the intrinsic spectrum and added together to give the emission spectra as in Equation (2). The EZ functions were normalized and multiplied by a factor for the device efficiencies at the different current densities. This factor and weights for the different EML positions were varied with the Solver tool in Excel to give a minimum RMS error for the fitting. First, all weights were allowed to vary individually in the fit to observe local minima solutions. To probe the existence of other minima, all practical EZ shapes (Figure S2, Supporting Information) were used as initial conditions. It was observed that a Gaussian function shape was the simplest function which fitted all the measurements of this study. Therefore, for computational efficiency, three parameters, the Gaussian width, position, and the device efficiency factor were varied for the EZ fits shown in the results. The resolution of the EZ functions was limited to quadratic function shapes across the EML, for this EML width.[8] The EML sampling distance of 3.9 nm (31 nm width/8 steps) was chosen as it was sufficient to map such quadratic order EZ functions. EZ solutions of higher resolution or spatial frequency could exist, however there was not sufficient optical resolution to see these. Nevertheless, the resulting solutions shown appear to be high enough resolution to see the charge balance trends in the device, as seen in Figure 2. The fitting was stopped when the RMS fitting error was equal to the experimental error.[26] This means that the fitting error will not be lower than the experimental error which would result in EZ solutions having spatial frequencies higher than the system resolution limit.[8] An example error analysis of the resulting EZ solutions is shown in Figure S17, Supporting Information. When the additional red spectral peak (originating from the HBL layer) appeared in the spectra, EZ fitting was performed over a limited wavelength range of 380 to 600 nm. The microcavity electric field plot in Figure 1 was simulated with the IMD software program.[49]

Device Experimental Characterization: The current density–voltage–luminance (*J*–*V*–*L*) characteristics and the external quantum efficiencies of the OLEDs were measured using an automatic IVL measurement system (ETS-170, System Engineers' Co., Ltd.) and a light distribution measurement system (C9920-11, Hamamatsu Photonics K. K.). The constant current density device lifetimes were measured using a lifetime measurement system (EAS-26, System Engineers' Co., Ltd.) and a Topcon SR-3AR spectroradiometer. Red emission from the HBL layer increased during lifetime measurements and this spectral change affects the calculated brightness. Therefore, for lifetime measurements, instead of using brightness, device spectra were instead integrated from 380 to 600 nm for each point in time to measure the radiance. Lifetimes agreed well for both the brightness and integrated partial spectra radiance for devices where the additional red emission was negligible. PLQYs were measured by a PLQY measurement system (Quantaurus-QY, Hamamatsu Photonics). The LUMO energy levels and the HOMO energy levels were taken from values in the literature.[4,5,33] For the charge de-trapping transient EL measurements shown in Figure S12, Supporting Information, pulsed voltages were applied using a function generator (WaveStation 2052, Teledyne Lecroy). The emitted light was detected using a photomultiplier tube (PMT) module (H10721-01, Hamamatsu Photonics) and the current signals from the PMT were amplified using a current amplifier (DHPCA-100, Femto). All signals were measured using an oscilloscope (HDO4054A, Teledyne Lecroy) with signal averaging performed over 5000 measurements.

Summary of the Advantages of the Introduced Single Emission Spectrum Method: For the single emission spectrum method, only a single 0° emission spectrum needed to be measured, with no additional loss-inducing optics such as linear polarizing filter or half wave plate necessary to deal with emitter orientation as in the conventional angular method. A precisely aligned rotation apparatus was also not required allowing for a simple measurement which was generally already measured for every LED device during research and development. This single emission spectrum measurement allowed tracking of the EZ with existing automated lifetime measurement setups, which was not easily compatible with the conventional angular measurement setup.

The single emission spectrum method EZ measurement took <1 s while the conventional angular method took several minutes to measure a single emission zone at a single current density. As a result, this method allowed the EZ to be measured for the full luminescing current density range and also gave the ability to observe fast device dynamics or minimize the effect of these dynamics at low (long time duration needed to get high enough emission spectrum signal) or high device driving.

A procedure was introduced to try to minimize charge balance changes and EZ changed between the thicker, EZ-sensitive dark device, and the thinner bright devices with maximum light outcoupling which were used in actual products. This involved transport layer engineering to have similar current voltage characteristics and a study to check if bright and dark devices had comparable EZs by comparing lifetime behavior while varying the device structure and ageing.

A method was outlined to show how to make a microcavity sensitive to all practical EZs and then verify this sensitivity. It was not illustrated before that a 10% deviation in the required thickness of the microcavity could lose EZ sensitivity. Error analysis to show the effect of microcavity thickness uncertainty on EZ center position is shown. A 1 nm accuracy of the microcavity thicknesses was shown to be achievable from a simple 0° emission spectrum measurement and then fitting with the simulation.

Fitting the unknown EZ as a single variable in the linear LED emission equation was introduced. Previously both the EZ and intrinsic spectrum were varied in the fitting process at the same time which could give erroneous results.

Statistical Analysis: Two devices were experimentally characterized (where possible) to show the repeatability of the results.

© 2022 The Authors. Advanced Materials published by Wiley-VCH GmbH

15214095, 2022, 29, Downloaded from https://onlinelibrary.wiley.com/doi/10.1002/adma.202201409 by EVIDENCE AID - BELGIUM, Wiley Online Library on [21/12/2022]. See the Terms and Conditions (https://onlinelibrary.wiley.com/terms-and-conditions) on Wiley Online Library for rules of use; OA articles are governed by the applicable Creative Commons License

Supporting Information

Supporting Information is available from the Wiley Online Library or from the author.

Acknowledgements

The authors are grateful for fruitful discussions on this manuscript with Jan Genoe, Karim Elkhouly, Iakov Goldberg, Laura Groeseneken, and Nirav Annavarapu. The authors acknowledge funding from the European Research Council under the European Horizon 2020 Program/ERC Grant Agreement No. 835133 (ULTRA-LUX) and the support of the Ministry of Education, Culture, Sports, Science and Technology (MEXT), Japan through the Program for Building Regional Innovation Ecosystems administered by Prof. R. Hayashi of Shibaura Institute of Technology, Tokyo.

Conflict of Interest

The authors declare no conflict of interest.

Author Contributions

R.M.C. conceived the study concept and the design of experiments. The research project was supervised by K.H., T.H.K., P.H., and C.A. R.M.C., K.N., and H.W.M. fabricated and characterized the devices. Data analysis and fitting was performed by R.M.C. Optical simulations were carried out by R.M.C. and R.G. R.M.C. wrote the manuscript. All authors discussed and gave input into the research progress and the manuscript.

Data Availability Statement

The data that support the findings of this study are available from the corresponding author upon reasonable request.

Keywords

degradation, device stability, emission zone, microcavities, organic light-emitting diodes, organic light-emitting diode charge dynamics, thermally activated delayed fluorescence

Received: February 12, 2022
Revised: May 7, 2022
Published online: June 12, 2022

[1] P. Nuss, M. J. Eckelman, *PLoS One* **2014**, *9*, e101298.
[2] D. Volz, M. Wallesch, C. Fléchon, M. Danz, A. Verma, J. M. Navarro, D. M. Zink, S. Bräse, T. Baumann, *Green Chem.* **2015**, *17*, 1988.
[3] C. Y. Chan, M. Tanaka, Y. T. Lee, Y. W. Wong, H. Nakanotani, T. Hatakeyama, C. Adachi, *Nat. Photonics* **2021**, *15*, 203.
[4] D. P. K. Tsang, T. Matsushima, C. Adachi, *Sci. Rep.* **2016**, *6*, 22463.
[5] H. Nakanotani, K. Masui, J. Nishide, T. Shibata, C. Adachi, *Sci. Rep.* **2013**, *3*, 2127.
[6] M. Flämmich, D. Michaelis, N. Danz, *Org. Electron.* **2011**, *12*, 83.
[7] S. L. M. Van Mensfoort, M. Carvelli, M. Megens, D. Wehenkel, M. Bartyzel, H. Greiner, R. A. J. Janssen, R. Coehoorn, *Nat. Photonics* **2010**, *4*, 329.
[8] N. Danz, R. MacCiarnain, D. Michaelis, T. Wehlus, A. F. Rausch, C. A. Wächter, T. C. G. Reusch, *Proc. SPIE* **2013**, *8829*, 882923.
[9] E. A. Silinsh, V. Gepak, in *Organic Molecular Crystals: Interaction, Localization and Transport Phenomena*, Vol. *2*, American Institute of Physics, New York **1994**, p. 169.
[10] N. C. Giebink, B. W. D'Andrade, M. S. Weaver, J. J. Brown, S. R. Forrest, *J. Appl. Phys.* **2009**, *105*, 124514.
[11] M. Tanaka, R. Nagata, H. Nakanotani, C. Adachi, *Commun. Mater.* **2020**, *1*, 18.
[12] N. Aizawa, A. Matsumoto, T. Yasuda, *Sci. Adv.* **2021**, *7*, 5769.
[13] Y. H. Lee, Y. S. Shin, T. Lee, J. Jung, J. H. Lee, M. H. Lee, *Chem. Eng. J.* **2021**, *423*, 130224.
[14] J. D. Lin, O. V. Mikhnenko, J. Chen, Z. Masri, A. Ruseckas, A. Mikhailovsky, R. P. Raab, J. Liu, P. W. Blom, M. A. Loi, C. J. Garcia-Cervera, *Mater. Horiz.* **2014**, *1*, 280.
[15] M. Jakoby, S. Heidrich, L. G. von Reventlow, C. Degitz, S. M. Suresh, E. Zysman-Colman, W. Wenzel, B. S. Richards, I. A. Howard, *Chem. Sci.* **2021**, *12*, 1121.
[16] M. Mesta, M. Carvelli, R. J. De Vries, H. Van Eersel, J. J. Van Der Holst, M. Schober, M. Furno, B. Lüssem, K. Leo, P. Loebl, R. Coehoorn, *Nat. Mater.* **2013**, *12*, 652.
[17] D. Y. Kondakov, *J. Appl. Phys.* **2008**, *104*, 084520.
[18] Y. Noguchi, H. J. Kim, R. Ishino, K. Goushi, C. Adachi, Y. Nakayama, H. Ishii, *Org. Electron.* **2015**, *17*, 184.
[19] Y. Zhang, J. Lee, S. R. Forrest, *Nat. Commun.* **2014**, *5*, 5008.
[20] A. Fakharuddin, W. Qiu, G. Croes, A. Devižis, R. Gegevičius, A. Vakhnin, C. Rolin, J. Genoe, R. Gehlhaar, A. Kadashchuk, V. Gulbinas, *Adv. Funct. Mater.* **2019**, *29*, 1904101.
[21] X. Dai, Z. Zhang, Y. Jin, Y. Niu, H. Cao, X. Liang, L. Chen, J. Wang, X. Peng, *Nature* **2014**, *515*, 96.
[22] Z. Zhang, Y. Ye, C. Pu, Y. Deng, X. Dai, X. Chen, D. Chen, X. Zheng, Y. Gao, W. Fang, X. Peng, *Adv. Mater.* **2018**, *30*, 1801387.
[23] S. K. Jeon, J. Y. Lee, *Org. Electron.* **2015**, *27*, 202.
[24] B. Sim, C. K. Moon, K. H. Kim, J. J. Kim, *ACS Appl. Mater. Interfaces* **2016**, *8*, 33010.
[25] B. Bailey, D. L. Farkas, D. L. Taylor, F. Lanni, *Nature* **1993**, *366*, 44.
[26] R. Mac Ciarnain, D. Michaelis, T. Wehlus, A. F. Rausch, N. Danz, A. Bräuer, A. Tünnermann, *Org. Electron.* **2017**, *44*, 115.
[27] M. Regnat, K. P. Pernstich, S. Züfle, B. Ruhstaller, *ACS Appl. Mater. Interfaces* **2018**, *10*, 31552.
[28] M. Regnat, K. P. Pernstich, K. H. Kim, J. J. Kim, F. Nüesch, B. Ruhstaller, *Adv. Electron. Mater.* **2020**, *6*, 1900804.
[29] M. C. Gather, M. Flämmich, N. Danz, D. Michaelis, K. Meerholz, *Appl. Phys. Lett.* **2009**, *94*, 263301.
[30] Y. H. Kim, C. Wolf, H. Kim, T. W. Lee, *Nano Energy* **2018**, *52*, 329.
[31] T. Zhang, C. Hu, S. Yang, *Small Methods* **2020**, *4*, 1900552.
[32] P. Wang, S. Zhao, Z. Xu, B. Qiao, Z. Long, Q. Huang, *Molecules* **2016**, *21*, 1365.
[33] M. Tanaka, H. Noda, H. Nakanotani, C. Adachi, *Adv. Electron. Mater.* **2019**, *5*, 1800708.
[34] H. S. Kim, S. R. Park, M. C. Suh, *J. Phys. Chem. C* **2017**, *121*, 13986.
[35] L. S. Cui, S. B. Ruan, F. Bencheikh, R. Nagata, L. Zhang, K. Inada, H. Nakanotani, L. S. Liao, C. Adachi, *Nat. Commun.* **2017**, *8*, 2250.
[36] K. Togashi, S. Nomura, N. Yokoyama, T. Yasuda, C. Adachi, *J. Mater. Chem.* **2012**, *22*, 20689.
[37] R. Mac Ciarnáin, H. W. Mo, K. Nagayoshi, H. Fujimoto, K. Harada, T. H. Ke, P. Heremans, C. Adachi, in *Proc. Int. Display Workshops*, Vol. *27*, ITE SID, Tokyo **2021**, p. 415.
[38] J. Kalinowski, *J. Non-Cryst. Solids* **2008**, *354*, 4170.
[39] A. S. Sandanayaka, T. Matsushima, C. Adachi, *J. Phys. Chem. C* **2015**, *119*, 23845.
[40] A. S. Sandanayaka, K. Yoshida, T. Matsushima, C. Adachi, *J. Phys. Chem. C* **2015**, *119*, 7631.
[41] K. Yamaguchi, T. Matsushima, A. S. Sandanayaka, Y. Homma, N. Uchida, C. Adachi, *Chem. - Eur. J.* **2020**, *26*, 5598.
[42] J. Sohn, D. Ko, H. Lee, J. Han, S. D. Lee, C. Lee, *Org. Electron* **2019**, *70*, 286.

© 2022 The Authors. Advanced Materials published by Wiley-VCH GmbH

15214095, 2022, 29, Downloaded from https://onlinelibrary.wiley.com/doi/10.1002/adma.202201409 by EVIDENCE AID - BELGIUM, Wiley Online Library on [21/12/2022]. See the Terms and Conditions (https://onlinelibrary.wiley.com/terms-and-conditions) on Wiley Online Library for rules of use; OA articles are governed by the applicable Creative Commons License

[43] T. Tsutsui, E. Aminaka, C. P. Lin, D. U. Kim, *Philos. Trans. R. Soc., A* **1997**, *355*, 801.
[44] H. Fujimoto, T. Nakamura, K. Nagayoshi, K. Harada, H. Miyazaki, T. Kurata, J. Kiyota, C. Adachi, *Appl. Phys. Lett.* **2020**, *116*, 143301.
[45] R. M. Ciarnáin, H. W. Mo, K. Nagayoshi, H. Fujimoto, K. Harada, T. H. Ke, P. Heremans, C. Adachi, *SID Int. Symp. Dig. Tech. Pap.* **2021**, *52*, 1477.
[46] Fluxim, Setfos version 5, https://www.fluxim.com (accessed: March 2022).
[47] J. W. Sun, J. H. Lee, C. K. Moon, K. H. Kim, H. Shin, J. J. Kim, *Adv. Mater.* **2014**, *26*, 5684.
[48] R. Mac Ciarnain, D. Michaelis, T. Wehlus, A. F. Rausch, S. Wehrmeister, T. D. Schmidt, W. Brütting, N. Danz, A. Bräuer, A. Tünnermann, *Sci. Rep.* **2017**, *7*, 1826.
[49] D. L. Windt, *Comput. Phys.* **1998**, *12*, 360.

© 2022 The Authors. Advanced Materials published by Wiley-VCH GmbH

15214095, 2022, 29, Downloaded from https://onlinelibrary.wiley.com/doi/10.1002/adma.202201409 by EVIDENCE AID - BELGIUM, Wiley Online Library on [21/12/2022]. See the Terms and Conditions (https://onlinelibrary.wiley.com/terms-and-conditions) on Wiley Online Library for rules of use; OA articles are governed by the applicable Creative Commons License